ADVANCES IN ATMOSPHERIC SCIENCES, VOL. 30, NO. 6, 2013, 1809–1820

Effects of Vertical Wind Shear, Radiation and Ice Microphysics on Precipitation Efficiency during a Torrential Rainfall Event in China

ZHOU Yushu (周玉淑)*

Laboratory of Cloud-Precipitation Physics and Severe Storms, Institute of Atmospheric Physics, Chinese Academy of Sciences, Beijing 100029

(Received 7 January 2013; revised 7 February 2013; accepted 25 February 2013)

ABSTRACT

The effects of vertical wind shear, radiation and ice microphysics on precipitation efficiency (PE) were investigated through analysis of modeling data of a torrential rainfall event over Jinan, China during July 2007. Vertical wind shear affected PE by changing the kinetic energy conversion between the mean and perturbation circulations. Cloud–radiation interaction impacted upon PE, but the relationship related to cloud radiative effects on PE was not statistically significant. The reduction in deposition processes associated with the removal of ice microphysics suppressed efficiency. The relationships related to effects of vertical wind shear, radiation and ice clouds on PEs defined in cloud and surface rainfall budgets were more statistically significant than that defined in the rain microphysical budget.

Key words: vertical wind shear, radiation, ice microphysics, precipitation efficiency

Citation: Zhou, Y. S., 2013: Effects of vertical wind shear, radiation and ice microphysics on precipitation efficiency during a torrential rainfall event in China. *Adv. Atmos. Sci.*, **30**(6), 1809–1820, doi: 10.1007/s00376-013-3007-1.

1. Introduction

Precipitation intensity is gauged by the surface rain rate, whereas the so-called precipitation efficiency (PE) is a measure of how efficiently rainfall sources, i.e. dynamic and thermodynamic processes as well as rain and cloud microphysical processes, are consumed to form precipitation. Generally, PE is defined by the ratio of the rain rate and the associated rainfall source. Sui et al. (2007) demonstrated that PE should be defined in a closed budget in which the rain rate is a term for which all the rainfall sources are properly counted and all the rainfall sinks are excluded, thus avoiding nonphysical values of PE, such as negative values and values of larger than 100%. Therefore, PE is budget dependent. For example, large-scale precipitation efficiency (LSPE) is defined in the surface rainfall budget (e.g. Auer and Marwitz, 1968; Heymsfield and Schotz, 1985; Chong and Hauser, 1989; Doswell et al., 1996), which originated from the first PE calculation by Braham (1952) who counted the inflow of water vapor into the precipitation system through the cloud base as the rainfall source. Later, with the development of precipitation modeling, the cloud-microphysics precipitation efficiency (CMPE) was defined in the cloud microphysical budget (e.g. Weisman and Klemp, 1982; Lipps and Hemler, 1986). Recently, Gao and Li (2011) defined the rain-microphysics precipitation efficiency (RMPE) in the rain microphysical budget, since rain microphysics is directly responsible for the production of precipitation. Gao and Li (2011) argued that RMPE is the "true" PE since rain microphysical processes are directly responsible for the production of rainfall and found a large difference between RMPE and LSPE. The three PE types are different because they are measured in different frameworks. From the derivations of surface rainfall and cloud and rain microphysical budgets, it is known that the rain microphysical budget is included in the cloud microphysical budget, which is then included in the surface rainfall budget. Thus, the rainfall source in the rain microphysical budget is a part of the rainfall source in the cloud microphysical

*Corresponding author: ZHOU Yushu, zys@mail.iap.ac.cn

budget, which in turn is a part of the rainfall source in the surface rainfall budget. Therefore, CMPE is larger than LSPE, but is smaller than RMPE.

The development of a precipitation system relies on many physical factors and processes, such as vertical wind shear (e.g. Wang et al., 2009b; Shen et al., 2011), radiation (e.g. Wang et al., 2010a; Shen et al., 2011) and ice clouds (e.g. Wang et al., 2010a, b). However, the effects of these on PE have not yet been studied. In the present reported work, sensitivity experiment data associated with a torrential rainfall event over Jinan, Shandong, China, during July 2007 from Zhou and Li (2011) were analyzed to investigate the effects of vertical wind shear, radiation and ice microphysics on PE. The model, experiment, forcing data, and definitions of PE are set out in the next section. The results are then presented in section 3, and a summary provided in section 4.

2. Model, experimental design, and definitions of PE

The sensitivity simulation data from Zhou and Li (2011) were analyzed in this study. It is important to note that the sensitivity experiments were carried out using a 2D cloud model because 2- and 3D cloud-resolving models produce similar cloud and rainfall simulations (e.g. Tao and Soong, 1986; Tao et al., 1987; Grabowski et al., 1998; Tompkins, 2000; Khairoutdinov and Randall, 2003; Sui et al., 2005). The same 2D cloud model was also used to simulate the surface rainfall processes associated with a torrential rainfall event over Hubei, China, during July 2007 (Zhou and Cui, 2011) and analyze thermally-related surface rainfall budgets associated with convective and stratiform rainfall (Zhou and Li, 2011). The model was integrated from 0200 LST 18 July to 1400 LST 19 July 2007 (a total of 36 hours) with forcing data averaged over a rectangular box of (113°–121°E, 36°–37°N) (Fig. 1), when severe weather and heavy rainfall developed near the Jinan area as a result of the interaction between a humid and warm air mass transported by a southwesterly jet and a dry and cold air mass transported by northerly winds from the northern regions of Lake Baikal (Zhou and Li, 2011). The rainfall simulation was validated by rain gauge observations as indicated by the calculation of the RMSE difference in surface rain rate between the simulation and observation (0.84 mm h^{-1}), which was lower than the standard deviation of the observed surface rain rate (1.10 mm h^{-1}). Zhou and Li (2011) carried out the control experiment (CTL) and four sensitivity experiments that excluded vertical wind shear (CNVWS), radiation (CNCR), cloud-radiation interaction (CNCRI) and ice microphysics (CNIM) (summarized in Table 1) to show the effects of these parameters on heavy rainfall. Thus, hourly grid-scale simulation data were analyzed in this study.

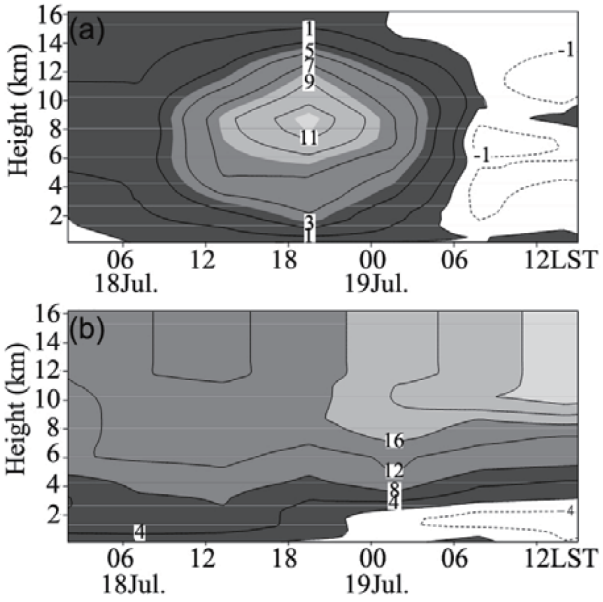

Fig. 1. Horizontal distributions of geopotential height (solid), temperature (dashed), and wind vector at 700 hPa on 1400 LST 18 Jul. 2007. Contour intervals are 20 m for geopotential height and 2°C for temperature.

The cloud resolving model used in Zhou and Li (2011) has five prognostic equations to predict mixing

Table 1. Summary of the sensitivity experiments.

Experiment	Vertical wind shear	Radiation	Ice microphysics
CTL	Yes	Yes	Yes
CNVWS	Mass-weighted mean zonal wind is imposed in the model	Yes	Yes
CNCR	Yes	No	Yes
CNCRI	Yes	Model domain mean vertical profile of radiation from CTL is imposed in the model	Yes
CNIM	Yes	Yes	No

ratios of cloud water, raindrops, cloud ice, snow, and graupel through single-moment cloud microphysical parameterization schemes, and also includes solar and thermal infrared radiation parameterization schemes to resolve cloud-radiation interaction processes. The model is furnished with cyclic lateral boundary conditions. The model setup also includes a model domain of 768 km with a horizontal grid mesh of 1.5 km, 33 vertical layers, and a time step of 12 s. This 2D model setup has been used to study tropical rainfall events (e.g. Li et al., 1999) and mid-latitude torrential rainfall events (e.g. Wang et al., 2009a; Shen et al., 2011). Detailed model descriptions, modeling, and analysis can be found in Li and Gao (2011) and Gao and Li (2011).

RMPE, CMPE and LSPE can be respectively defined as

$$\mathrm{RMPE} = \frac{P_\mathrm{S}}{\mathrm{RSRB}}, \tag{1a}$$

$$\mathrm{CMPE} = \frac{P_\mathrm{S}}{\mathrm{RSCB}}, \tag{1b}$$

$$\mathrm{LSPE} = \frac{P_\mathrm{S}}{\mathrm{RSWVCB}}, \tag{1c}$$

where

$$\mathrm{RSRB} = \sum_{\mathrm{PI}=1}^{12} H(R_\mathrm{PI})R_\mathrm{PI} + H(Q_\mathrm{RM})Q_\mathrm{RM}\ , \tag{2a}$$

$$\mathrm{RSCB} = \sum_{I=1}^{7} H(S_I)S_I + H(Q_\mathrm{CM})Q_\mathrm{CM}\ , \tag{2b}$$

$$\mathrm{RSWVCB} = H(Q_\mathrm{WVT})Q_\mathrm{WVT} + H(Q_\mathrm{WVF})Q_\mathrm{WVF} + H(Q_\mathrm{WVE})Q_\mathrm{WVE} + H(Q_\mathrm{CM})Q_\mathrm{CM}\ , \tag{2c}$$

$$\begin{aligned} R_\mathrm{PI} = \{&[P_\mathrm{SACW}(T>T_0)], [P_\mathrm{RAUT}], [P_\mathrm{RACW}]\ , [P_\mathrm{GACW}(T>T_0)], -[P_\mathrm{REVP}], [P_\mathrm{RACS}(T>T_0)]\ , \\ &-[P_\mathrm{IACR}(T<T_0)], -[P_\mathrm{GACR}(T<T_0)]\ , -[P_\mathrm{SACR}(T<T_0)], -[P_\mathrm{GFR}(T<T_0)]\ , \\ &[P_\mathrm{SMLT}(T>T_0)], [P_\mathrm{GMLT}(T>T_0)]\}\ , \end{aligned} \tag{2d}$$

$$\begin{aligned} S_\mathrm{I} = ([&P_\mathrm{CND}], [P_\mathrm{DEP}], [P_\mathrm{SDEP}], [P_\mathrm{GDEP}], \\ &-[P_\mathrm{REVP}], -[P_\mathrm{MLTG}], -[P_\mathrm{MLTS}]), \end{aligned} \tag{2e}$$

$$Q_\mathrm{RM} = -\frac{\partial[q_\mathrm{r}]}{\partial t} - \left[u\frac{\partial q_\mathrm{r}}{\partial x}\right] - \left[w\frac{\partial q_\mathrm{r}}{\partial z}\right]\ , \tag{2f}$$

$$Q_\mathrm{CM} = -\frac{\partial[q_\mathrm{l}]}{\partial t} - \left[u\frac{\partial q_\mathrm{l}}{\partial x}\right] - \left[w\frac{\partial q_\mathrm{l}}{\partial z}\right]\ , \tag{2g}$$

$$Q_\mathrm{WVT} = -\frac{\partial[q_\mathrm{v}]}{\partial t}, \tag{2h}$$

$$\begin{aligned} Q_\mathrm{WVF} = &-\left[\bar{u}_\mathrm{o}\frac{\partial \bar{q}_\mathrm{v,o}}{\partial x}\right] - \left[\bar{w}_\mathrm{o}\frac{\partial \bar{q}_\mathrm{v}}{\partial z}\right] - \left[\bar{w}_\mathrm{o}\frac{\partial q'_\mathrm{v}}{\partial z}\right] \\ &-\left[w'\frac{\partial \bar{q}_\mathrm{v}}{\partial z}\right] - \left[\frac{\partial}{\partial x}(\bar{u}_\mathrm{o}+u')q'_\mathrm{v}\right]\ , \end{aligned} \tag{2i}$$

$$Q_\mathrm{WVE} = E_\mathrm{s}\ . \tag{2j}$$

Here, P_S is the surface rain rate; u and w are the zonal and vertical components of wind, respectively; R_PI denotes rainfall source/sink terms from rain microphysical processes; and S_I denotes rainfall source/sink terms from cloud microphysical processes, which are defined in Li and Gao (2011). For the Eqs. (1a–1c) and microphysical processes represented by Eqs. (2c)–(2e), see Gao and Li (2011). q_v is specific humidity; $q_\mathrm{l} = q_\mathrm{c} + q_\mathrm{r} + q_\mathrm{i} + q_\mathrm{s} + q_\mathrm{g}$, where $q_\mathrm{c}, q_\mathrm{r}, q_\mathrm{i}, q_\mathrm{s}, q_\mathrm{g}$ are the mixing ratios of cloud water, raindrops, cloud ice, snow, and graupel, respectively; E_s is the surface evaporation rate; and T_0 means the temperature equals zero, namely, $T_0 = 0°\mathrm{C}$. Overbars represent the domain mean, and primes the perturbation from the domain mean; subscript "$\circ$" denotes imposed observed large-scale variables in the model; and

$$[()] = \int_{z_\mathrm{b}}^{z_\mathrm{t}} \bar{\rho}()dz\ ,$$

with z_t and z_b being the heights of the top and bottom of the model atmosphere, respectively. RSRB, RSCB and RSWVCB are the rainfall sources from rain, cloud and surface rainfall budgets, respectively. H is the Heaviside function, $H(F) = 1$ when $F > 0$, and $H(F) = 0$ when $F \leqslant 0$. The rainfall sources used to compute precipitation efficiencies are calculated by accumulating rainfall sources from each model grid over the model domain each hour.

3. Results Analyses

The control experiment and CNVWS showed similar RMPEs and CMPEs, whereas LSPE was larger in CNVWS than in CTL (Fig. 2). The exclusion of vertical wind shear may enhance LSPE. RMPE was larger in CNCR than in CTL when RMPE was smaller than 40%, but both experiments showed similar RMPEs when RMPE was larger than 40%. CNCR tended to have a larger CMPE than the control experiment, especially for smaller CMPEs. LSPE was generally larger in CNCR than in CTL, implying that the exclusion of cloud radiative effects leads to larger PEs. The

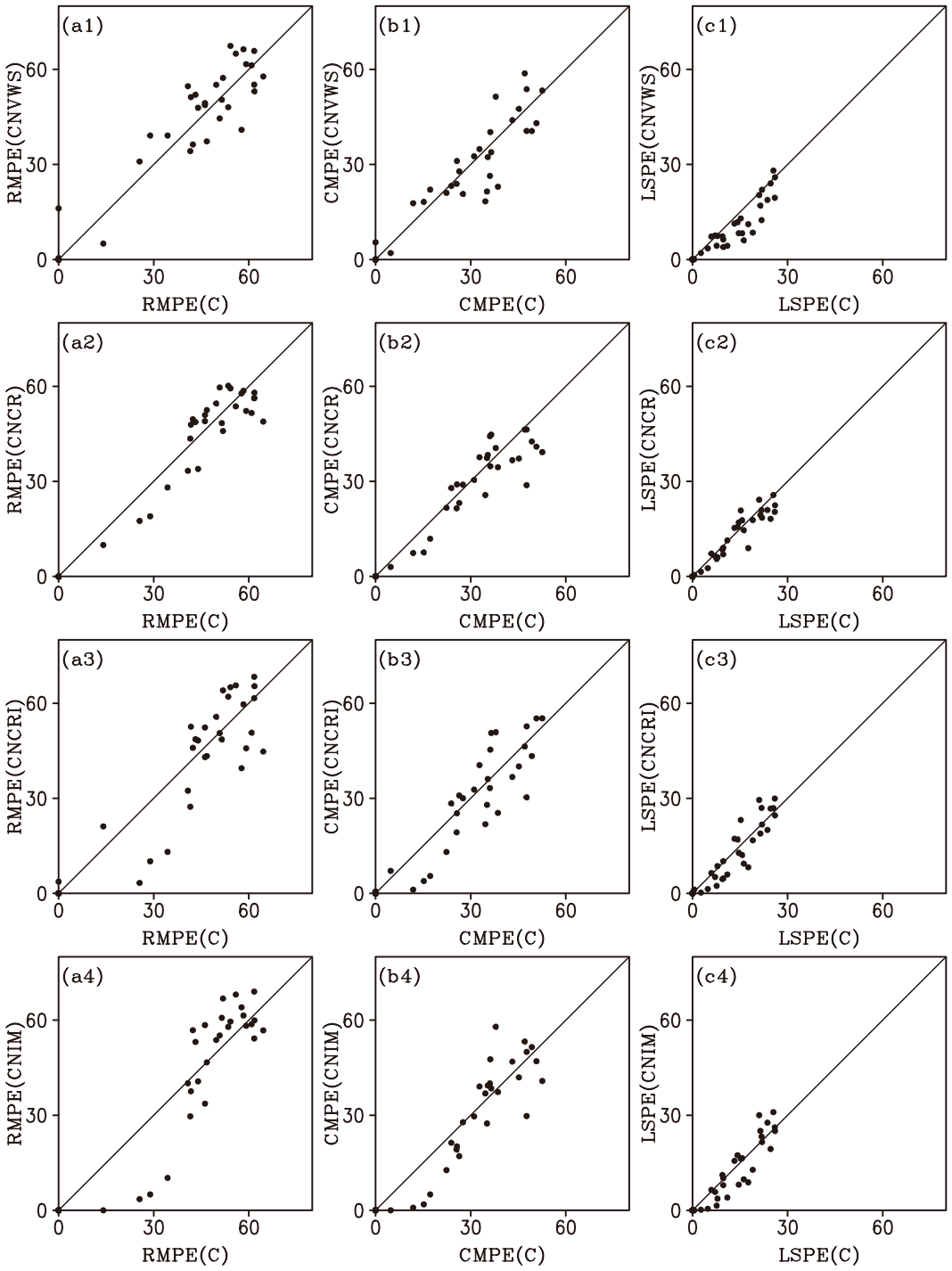

Fig. 2. (a) RMPE in sensitivity experiments vs. RMPE in CTL; (b) CMPE in sensitivity experiments vs. CMPE in CTL; and (c) LSPE in sensitivity experiments vs. LSPE in CTL. Numbers 1, 2, 3 and 4 denote sensitivity experiments CNVWS, CNCR, CNCRI and CNIM, respectively. Units: %.

control experiment and CNCRI showed similar large PEs, but the PEs were larger in CNCRI than in CTL for small PEs, suggesting that cloud–radiation interaction may affect smaller PEs. PEs were generally larger in CNIM than in CTL for large PEs, whereas they were smaller in CNIM than in CTL for small PEs, indicat-

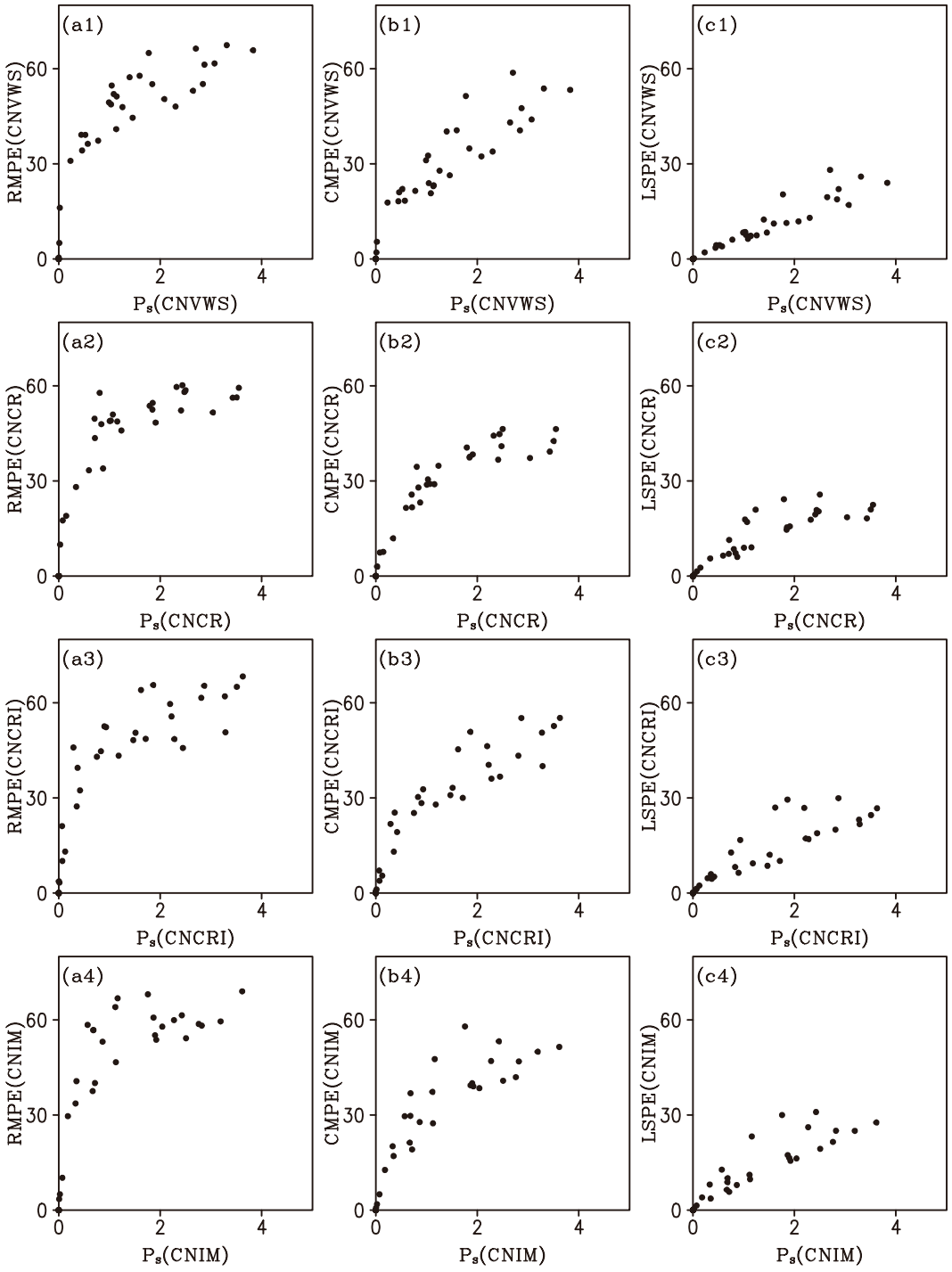

Fig. 3. (a) RMPE in sensitivity experiments versus P_S in CTL; (b) CMPE in sensitivity experiments vs. P_S in CTL; and (c) LSPE in sensitivity experiments versus P_S in CTL. Numbers 1, 2, 3 and 4 denote sensitivity experiments CNVWS, CNCR, CNCRI and CNIM, respectively. Units are % for RMPE, CMPE, and LSPE, and mm h^{-1} for P_S.

ing that the exclusion of ice clouds enhances small PEs but suppresses large PEs.

Since PE is defined as the ratio of rain rate to all rainfall sources, it was proportional to the rain rate as indicated in Fig. 3; all the PEs increased as the rain rate increased. The differences in PEs between sensi-

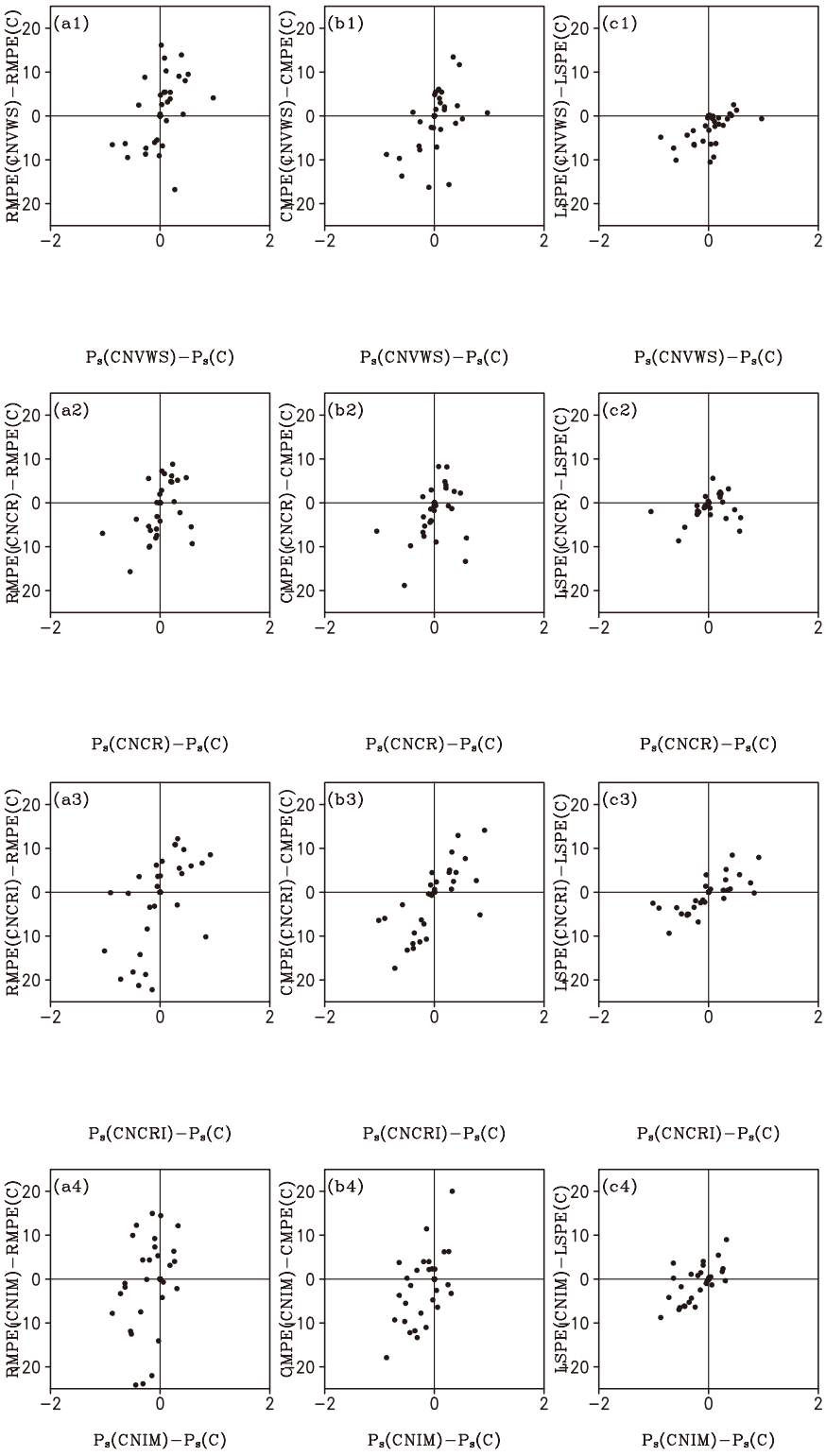

Fig. 4. Differences in (a) RMPE, (b) CMPE, and (c) LSPE between sensitivity experiments and CTL vs. differences in P_S between sensitivity experiments and CTL. Numbers 1, 2, 3 and 4 denote sensitivity experiments CNVWS, CNCR, CNCRI and CNIM, respectively. Units are % for RMPE, CMPE, and LSPE, and mm h^{-1} for P_S.

Table 2. Linear correlation coefficients of differences in PEs between the sensitivity experiments and the control experiment with differences in rain rates. The correlation coefficients that were larger than the critical correlation coefficient are marked bold.

	Diff. in RMPE	Diff. in CMPE	Diff. in LSPE
Diff. in P_S for CNVWS-CTL	**0.43**	**0.48**	**0.54**
Diff. in P_S for CNCR-CTL	**0.42**	**0.35**	0.25
Diff. in P_S for CNCRI-CTL	**0.56**	**0.72**	**0.74**
Diff. in P_S for CNIM-CTL	0.33	**0.55**	**0.64**

tivity experiments and the control experiment versus the differences in rain rates in Fig. 4 further showed linear correlations. Student's t-tests on the significance of the correlation coefficients were conducted and the critical correlation coefficient at the 5% significant level was 0.33. Calculations of linear correlation coefficients showed that most of the linear relationships were statistically significant (Table 2). Thus, the effects of vertical wind shear, radiation, and ice microphysics on PE could be studied through analysis of the rainfall responses to these physical processes and factors.

Vertical wind shear may affect rainfall by changing the barotropic conversion $[C(\overline{K}, K')]$ between mean kinetic energy $(\overline{K})$ and perturbation kinetic energy (K') as secondary circulation is directly responsible for the production of rainfall, which is measured by perturbation kinetic energy (Wang et al., 2009b; Shen et al., 2011; Zhou and Li, 2011). $C(\overline{K}, K')$ can be expressed by

$$C(\bar{K}, K') = -\left[\overline{u'w'}\frac{\partial \bar{u}_o}{\partial z}\right] . \quad (3)$$

Thus, the conversion is determined by the covariance between the perturbation zonal wind (u') and the vertical velocity (w') under vertical shear of the imposed zonal wind $(\partial \bar{u}_o/\partial z)$. The difference in rain rate between CNVWS and CTL was positively correlated, with a coefficient of 0.45 (Fig. 5a). The conversion vanishes for CNVWS due to the exclusion of vertical wind shear. The positive correlation implies that rainfall increases as conversion from mean kinetic energy to perturbation kinetic energy increases. As a result, the differences in precipitation efficiencies between CNVWS and CTL were positively correlated with the differences in kinetic energy conversion (Figs. 6a1–c1 and Table 3). Note that the correlation coefficients for RMPE and LSPE only marginally exceeded the critical correlation coefficient (Table 3). The vertical profiles of imposed large-scale zonal wind were averaged for $C(\overline{K}, K') > 0$ and $C(\overline{K}, K') < 0$, respectively. The positive vertical shear of zonal wind from 2 km to 10 km was weaker for $C(\overline{K}, K') > 0$ than for $C(\overline{K}, K') < 0$ (Fig. 7). Below 2 km, vertical shear of zonal wind was positive for $C(\overline{K}, K') > 0$ but negative for $C(\overline{K}, K') < 0$.

The difference in the mean radiation (S_{RAD}) was generally negative, indicating that the exclusion of cloud radiative effects increases the mean radiative cooling. The difference in the mean radiative cooling between CNCR and CTL was calculated and their linear correlation with the differences in the rain rate between CNCR and CTL analyzed. Figure 5b shows a negatively linear correlation with a coefficient of −0.20, which is statistically insignificant. This insignificant negative correlation led to statistically insignificant negative correlations between the differences in the PEs for CNCR-CTL and the difference in S_{RAD} (Figs. 6a2–c2). Although statistically insignificant, the negative correlation suggests that the rain rate may increase as the radiative cooling increases.

The exclusion of cloud–radiation interaction was able to increase or decrease the mean latent heat and

Table 3. Linear correlation coefficients of differences in PEs between sensitivity experiments and the control experiment with $C(\overline{K}, K')$ for CNVWS-CTL, S_{RAD} for CNCR-CTL, and S_{LH} for CNCRI-CTL and CNIM-CTL. The correlation coefficients that were larger than the critical correlation coefficient are marked bold.

	Diff. in RMPE	Diff. in CMPE	Diff. in LSPE
Diff. in $C(\overline{K}, K')$ for CNVWS-CTL	**0.37**	**0.46**	**0.35**
Diff. in S_{RAD} for CNCR-CTL	−0.01	−0.08	−0.07
Diff. in S_{LH} for CNCRI-CTL	**0.49**	**0.67**	**0.65**
Diff. in S_{LH} for CNIM-CTL	0.23	**0.59**	**0.58**

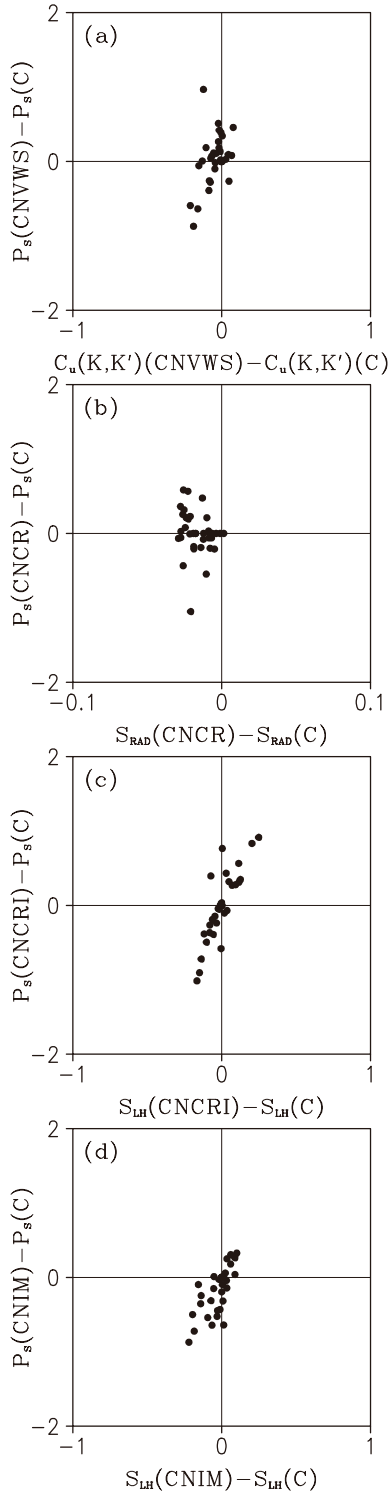

Fig. 5. (a) Difference in P_S (mm h^{-1}) between CNVWS and CTL vs. difference in $C(\overline{K}, K')$ (10^7 J s^{-1}); (b) difference in P_S between CNCR and CTL vs. difference in S_{RAD} (°C h^{-1}); (c) difference in P_S between CNCRI and CTL vs. difference in S_{LH} (°C h^{-1}); and (d) difference in P_S between CNVWS and CTL vs. difference in S_{LH}.

thus the rain rate (Fig. 5c), as indicated by the linear correlation coefficient of 0.85. The high degree of linear correlation between the rainfall and latent heat (S_{LH}) differences for CNCRI-CTL led to the statistically significant linear correlation between the differences in PEs and latent heat (Figs. 6a3–c3 and Table 3). The linear correlation coefficient between the RMPE and latent-heat differences was smaller than those between the CMPE and latent-heat differences and between the LSPE and latent-heat differences. The effects of cloud–radiation interaction on heat balance can be analyzed through the difference in heat budget between CNCRI and C. The mass-weighted mean heat budget can be written as

$$S_{HT} + S_{HF} + S_{HS} + S_{LH} + S_{RAD} = 0\,, \qquad (4)$$

where

$$S_{HT} = -\frac{\partial\langle\overline{T}\rangle}{\partial t}\,, \qquad (4a)$$

$$S_{HF} = -\left\langle \bar{u}_o \frac{\partial \overline{T}_o}{\partial x}\right\rangle - \left\langle \pi\bar{w}_o \frac{\partial\bar{\theta}}{\partial z}\right\rangle\,, \qquad (4b)$$

$$S_{HS} = \overline{F}_S\,, \qquad (4c)$$

$$S_{LH} = \frac{1}{c_p}\langle\overline{Q}_{cn}\rangle\,, \qquad (4d)$$

$$S_{RAD}\frac{1}{c_p}\langle\overline{Q}_R\rangle. \qquad (4e)$$

Here, T and θ are air temperature and potential temperature, respectively; c_p is the specific heat of dry air at constant pressure; $\overline{F}_S$ is surface sensible heat flux; Q_{cn} denotes the net latent heat release through phase changes among water vapor and cloud species; Q_R is the radiative heating rate due to the convergence of net flux of solar and infrared radiative fluxes, and

$$\langle()\rangle = \int_{z_b}^{z_t}\bar{\rho}()dz \Big/ \int_{z_b}^{z_t}\bar{\rho}dz\,.$$

Heat budget [(Eq. (4)] states that the local heat change (S_{HT}) is determined by heat divergence (S_{HF}), surface sensible heat flux (S_{HS}), latent heat release (S_{LH}) and radiation (S_{RAD}). Figure 8a shows that the difference in S_{LH} for CNCRI-CTL was negatively correlated with the difference in S_{HT}. This implies that the local heat change is associated with the latent-heat response to the cloud–radiation interaction.

The removal of ice microphysics could enhance or suppress latent heat and thus the rain rate (Fig. 5d), and the linear correlation coefficient between the rainfall and latent-heat differences for CNIM-CTL was 0.72, which far exceeded the critical correlation coefficient. The difference in the latent heat for CNIM-CTL was linearly correlated with the differences in CMPE and LSPE, but was not well correlated with the difference in RMPE (Figs. 6a4–c4 and Table 3). The ex-

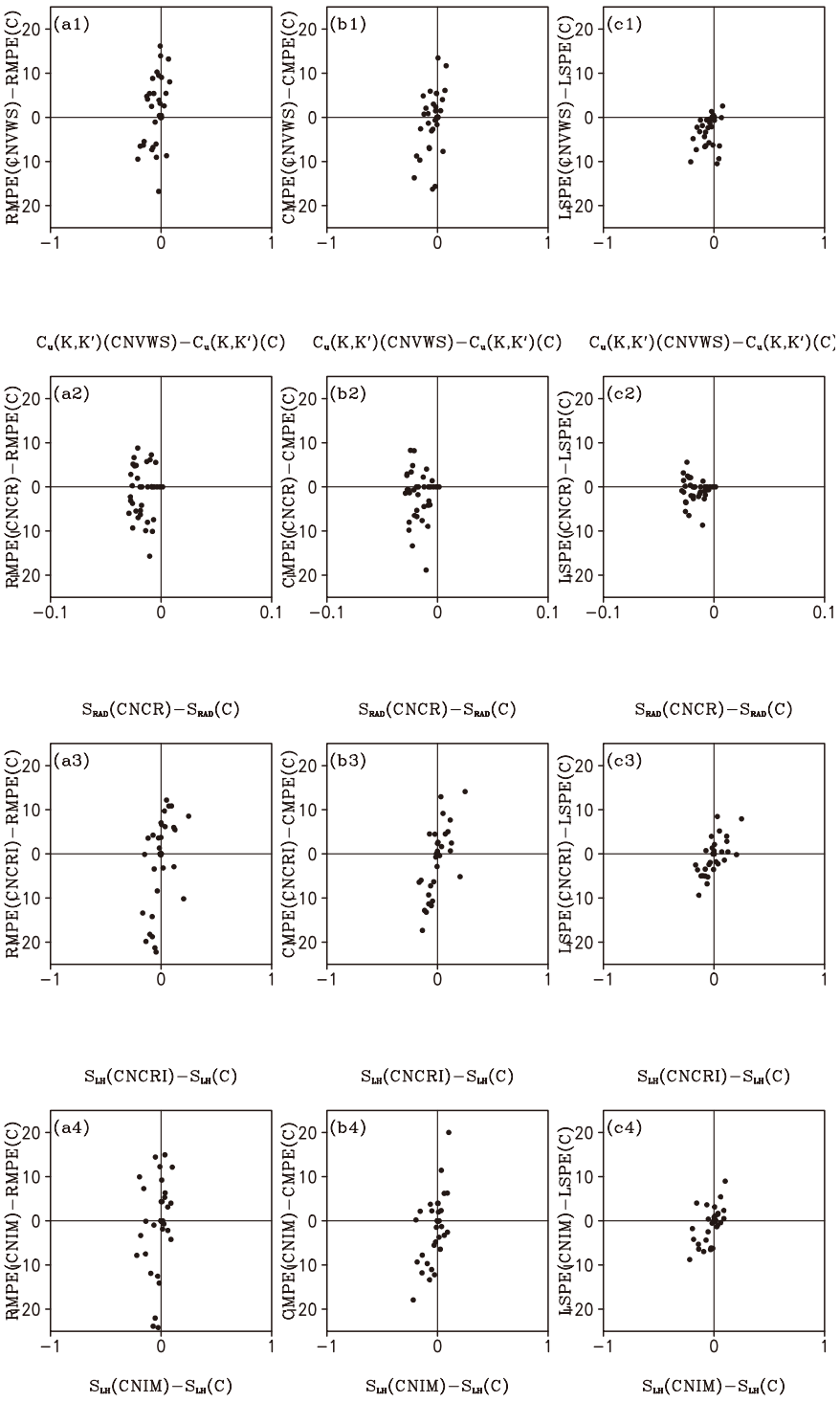

Fig. 6. Differences in (a1) RMPE (%), (b1) CMPE (%) and (c1) LSPE(%) between CNVWS and CTL vs. differences in $C(\overline{K}, K')$ (10^7 J s^{-1}); differences in (a2) RMPE (%), (b2) CMPE (%) and (c2) LSPE(%) between CNCR and CTL vs. differences in $S_{\rm RAD}$ (°C h^{-1}); differences in (a3) RMPE (%), (b3) CMPE (%) and (c3) LSPE(%) between CNCRI and CTL vs. differences in $S_{\rm LH}$ (°C h^{-1}); and differences in (a4) RMPE (%), (b4) CMPE (%) and (c4) LSPE(%) between CNIM and CTL vs. differences in $S_{\rm LH}$ (°C h^{-1}).

clusion of ice microphysics reduced the latent heat release associated with vapor condensation and deposition rate, and also changed the latent heat related to the evaporation of precipitation hydrometeors. The positive difference in $S_{\rm LH}$ from CTL to CNIM demonstrates that the reduction in the latent heat associated with evaporation was larger than the reduction in the latent heat associated with condensation and deposition. Figure 8b reveals that the difference in $S_{\rm LH}$ was negatively correlated with $S_{\rm HF}$. This suggests that the difference in heat divergence between CNIM and C mainly corresponds to the difference in the latent heat caused by the elimination of ice microphysics.

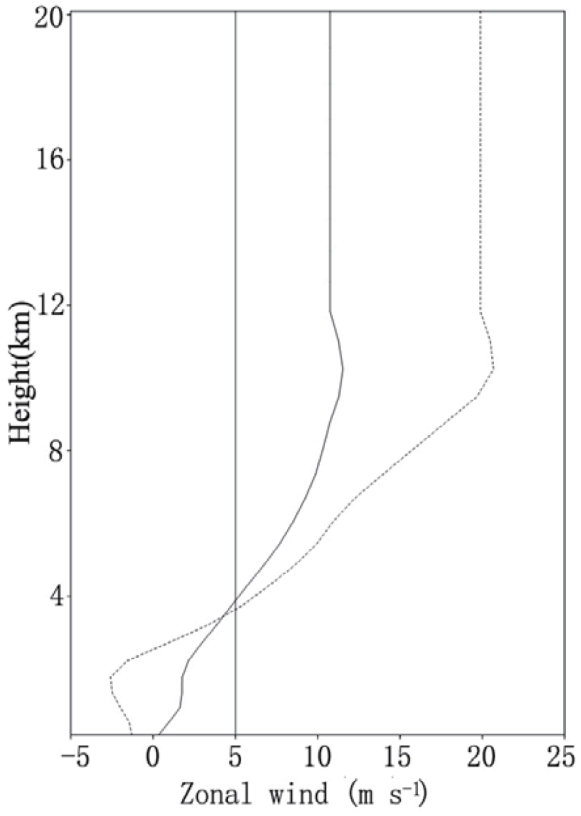

Fig. 7. Vertical profiles of imposed large-scale zonal wind (m s^{-1}) averaged for $C(\overline{K}, K') > 0$ (solid) and $C(\overline{K}, K') < 0$ (dashed).

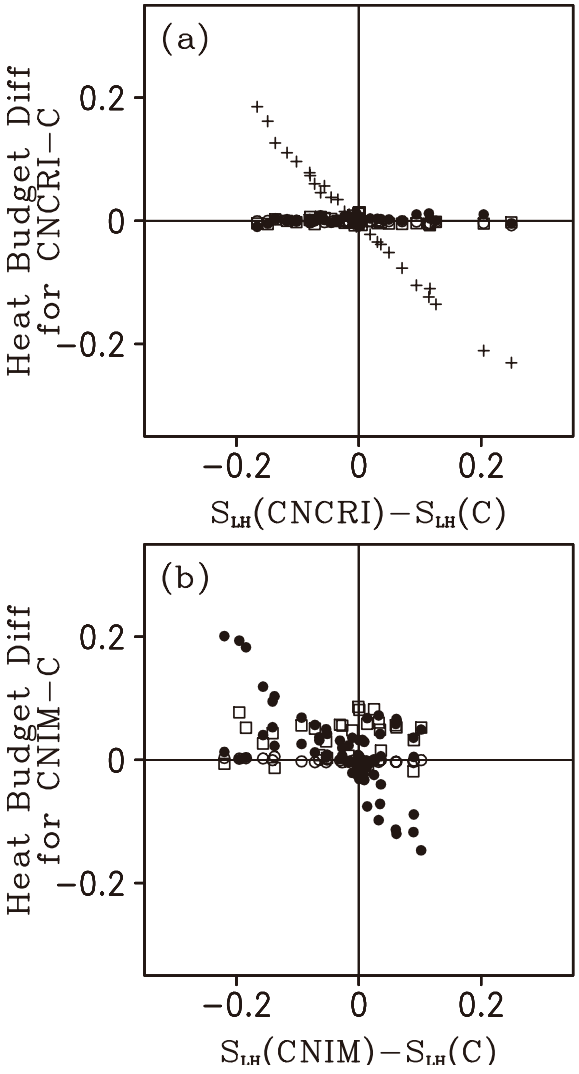

Fig. 8. Differences in $S_{\rm LH}$ vs. differences in other terms in mass-weighted mean heat budget [$S_{\rm HT}$ (crosses), $S_{\rm HS}$ (open circles), $S_{\rm HF}$ (closed circles), and $S_{\rm RAD}$ (open squares)] for (a) CNCRI-CTL and (b) CNIM-CTL. Units: °C h^{-1}.

4. Summary

The effects of vertical wind shear, radiation, and ice microphysics on PE associated with torrential rainfall over Jinan, Shandong, China, during 18–19 July 2007 were examined in this study. A series of sensitivity cloud-resolving model experiments forced by National Centers for Environmental Prediction (NCEP)/Global Data Assimilation System (GDAS) data from Zhou and Li (2011) were analyzed. Three PEs were defined; namely, RMPE in the rain microphysical budget, CMPE in the cloud microphysical budget, and LSPE in the surface rainfall budget. The major results can be summarized as:

(1) Vertical wind shear affected PE by changing conversion between the mean kinetic energy and perturbation kinetic energy as the rainfall was linked to secondary circulation. PE increased as the mean kinetic energy was converted into perturbation kinetic energy by relatively weak positive vertical wind shear. The correlation between CMPE and the vertical wind shear was more statistically significant than those of

RMPE and LSPE.

(2) A statistically significant relationship related to cloud radiative effects on PE could not be established for this torrential rainfall case since the variation in radiation resulting from the exclusion of cloud radiative effects could not account for the variation in rainfall.

(3) Cloud–radiation interaction impacted upon PE via changing net latent heat. The correlation between the differences of RMPE and net latent heat caused by the removal of cloud–radiation interaction was less statistically significant than those of CMPE and LSPE.

(4) Ice microphysics affected PE through a change in net latent heat. The reduction in net latent heat due to the exclusion of deposition processes led to a decrease in PE. The relationship related to the effects of ice microphysics on RMPE was not statistically significant.

Acknowledgements. The author thanks Dr. W.-K. TAO at NASA/GSFC for his 2D cloud-resolving model. This study was supported by projects of the National Natural Sciences Foundation of China (Grant Nos. 41075044, 41275065, and 41075079).

REFERENCES

Auer, A. H. Jr., and J. D. Marwitz, 1968: Estimates of air and moisture flux into hailstorms on the High Plains. *J. Appl. Meteor.*, **7**(2), 196–198.

Braham, R. R. Jr., 1952: The water and energy budgets of the thunderstorm and their relation to thunderstorm development. *J. Meteor.*, **9**(4), 227–242.

Chong, M., and D. Hauser, 1989: A tropical squall line observed during the CORT 81 experiment in West Africa. Part II: Water budget. *Mon. Wea. Rev.*, **117**(4), 728–744.

Doswell, C. A., III, H. E. Brooks, and R. A. Maddox, 1996: Flash flood forecasting: An ingredients-based methodology. *Wea. Forecasting*, **11**(4), 560–581.

Gao, S., and X. Li, 2011: Can water vapor process data be used to estimate precipitation efficiency? *Quart. J. Roy. Meteor. Soc.*, **137**(657), 969–978, doi:10.1002/qj.806.

Grabowski, W. W., X. Wu, M. W. Moncrieff, and W. D. Hall, 1998: Cloud-resolving model of tropical cloud systems during Phase III of GATE. Part II: Effects of resolution and the third spatial dimension. *J. Atmos. Sci.*, **55**(21), 3264–3282.

Heymsfield, G. M., and S. Schotz, 1985: Structure and evolution of a severe squall line over Oklahoma. *Mon. Wea. Rev.*, **113**(9), 1563–1589.

Khairoutdinov, M. F., and D. A. Randall, 2003: Cloud-resolving modeling of the ARM summer 1997 IOP: Model formulation, results, uncertainties, and sensitivities. *J. Atmos. Sci.*, **60**(4), 607–625.

Li, X., and S. Gao, 2011: *Precipitation Modeling and Quantitative Analysis*. Springer, Dordrecht. 240pp.

Li, X., C.-H. Sui, K.-M. Lau, and M.-D. Chou, 1999: Large-scale forcing and cloud-radiation interaction in the tropical deep convective regime. *J. Atmos. Sci.*, **56**(17), 3028–3042.

Lipps, F. B., and R. S. Hemler, 1986: Numerical simulation of deep tropical convection associated with large-scale convergence. *J. Atmos. Sci.*, **43**(17), 1796–1816.

Shen, X., Y. Wang, and X. Li, 2011: Effects of vertical wind shear and cloud radiatve processes on responses of rainfall to the large-scale forcing during pre-summer heavy rainfall over southern China. *Quart. J. Roy. Meteor. Soc.*, **137**(654), 236–249.

Sui, C.-H., X. Li, M.-J. Yang, and H.-L. Huang, 2005: Estimation of oceanic precipitation efficiency in cloud models. *J. Atmos. Sci.*, **62**(12), 4358–4370.

Sui, C.-H., X. Li, and M.-J. Yang, 2007: On the definition of precipitation efficiency. *J. Atmos. Sci.*, **64**(12), 4506–4513, doi:10.1175/2007jas2332.1.

Tao, W.-K., and S.-T. Soong, 1986: The study of the response of deep tropical clouds to mesoscale processes: Three-dimensional numerical experiments. *J. Atmos. Sci.*, **43**(22), 2653–2676.

Tao, W.-K., J. Simpson, and S.-T. Soong, 1987: Statistical properties of a cloud ensemble: A numerical study. *J. Atmos. Sci.*, **44**(21), 3175–3187.

Tompkins, A. M., 2000: The impact of dimensionality on long-term cloud-resolving model simulations. *Mon. Wea. Rev.*, **128**(5), 1521–1535.

Wang, D., X. Li, W.-K. Tao, Y. Liu, and H. Zhou, 2009a: Torrential rainfall processes associated with a landfall of severe tropical strom Bilis (2006): A two-dimensional cloud-resolving modeling study. *Atmospheric Research*, **91**(1), 94–104.

Wang, D., X. Li, W.-K. Tao, and Y. Wang, 2009b: Effects of vertical wind shear on convective development during a landfall of severe tropical storm Bilis (2006). *Atmospheric Research*, **94**(2), 270–275.

Wang, D., X. Li, and W.-K. Tao, 2010a: Cloud radiative effects on responses of rainfall to large-scale forcing during a landfall of severe tropical storm Bilis (2006). *Atmospheric Research*, **98**(2), 512–525.

Wang, D., X. Li, and W.-K. Tao, 2010b: Torrential rainfall responses to radiative and microphysical processes of ice clouds during a landfall of severe tropical storm Bilis (2006). *Meteor. Atmos. Phys.*, **109**(3), 115–128.

Weisman, M. L., and J. B. Klemp, 1982: The dependence of numerically simulated convective storms on vertical wind shear and buoyancy. *Mon. Wea. Rev.*, **110**(6), 504–520.

Zhou, Y, 2011: Effects of vertical wind shear, radiation, and ice clouds on a torrential rainfall event over Jinan, China in July 2007. *J. Geophys. Res.*, **116**(D5), D05118, doi:10.1029/2010JD014518.

Zhou, Y. S., and C. G. Cui, 2011: A modeling study of surface rainfall processes associated with a torrential rainfall event over Hubei, China, during

July 2007. *Adv. Atmos. Sci.*, **28**(6), 1459–1470, doi: 10.1007/s00376-010-0119-8.

Zhou, Y. S., and X. F. Li, 2011: An analysis of thermally-related surface rainfall budgets associated with convective and stratiform rainfall. *Adv. Atmos. Sci.*, **28**(5), 1099–1108, doi: 10.1007/s00376-010-0031-2.